Navigator

NAVO MSRC SPRING 2004

News and information from...

The Naval Oceanographic Office Major Shared Resource Center

Report Documentation Page

Form Approved
OMB No. 0704-0188

1. REPORT DATE	2. REPORT TYPE	3. DATES COVERED
2004		**00-00-2004 to 00-00-2004**

4. TITLE AND SUBTITLE	5a. CONTRACT NUMBER
NAVO MSRC Navigator. Spring 2004	5b. GRANT NUMBER
	5c. PROGRAM ELEMENT NUMBER
6. AUTHOR(S)	5d. PROJECT NUMBER
	5e. TASK NUMBER
	5f. WORK UNIT NUMBER
7. PERFORMING ORGANIZATION NAME(S) AND ADDRESS(ES) **Naval Oceanographic Office (NAVO),Major Shared Resource Center (MSRC),1002 Balch Boulevard,Stennis Space Center,MS,39522**	8. PERFORMING ORGANIZATION REPORT NUMBER
9. SPONSORING/MONITORING AGENCY NAME(S) AND ADDRESS(ES)	10. SPONSOR/MONITOR'S ACRONYM(S)
	11. SPONSOR/MONITOR'S REPORT NUMBER(S)

12. DISTRIBUTION/AVAILABILITY STATEMENT
Approved for public release; distribution unlimited

13. SUPPLEMENTARY NOTES

14. ABSTRACT

15. SUBJECT TERMS

16. SECURITY CLASSIFICATION OF:			17. LIMITATION OF ABSTRACT	18. NUMBER OF PAGES	19a. NAME OF RESPONSIBLE PERSON
a. REPORT	b. ABSTRACT	c. THIS PAGE			
unclassified	**unclassified**	**unclassified**	**Same as Report (SAR)**	**28**	

Steve Adamec, NAVO MSRC Director

NAVO MSRC System Upgrades Support Users

Significant enhancements to the NAVO MSRC computing capability are on the way this spring and summer, thanks to the Technology Insertion for FY04 (TI-04) upgrades that were recently approved by our sponsors.

These enhancements include substantial upgrades to the MSRC High Performance Computing (HPC) systems configuration, the Remote Storage Facility (RSF), and the internal MSRC networking capability.

When the TI-04 upgrades are complete, they will provide almost 30 teraflops of aggregate peak computing capability with commensurately balanced storage and networking capabilities—including the installation of one of the world's most capable HPC systems, a 2944-processor IBM POWER4+ system. This enormous computational capability will continue to enable unparalleled advances in the DoD science and technology areas served by the HPC Modernization Program (HPCMP).

As I've mentioned in past issues of *The Navigator*, we recognize that it is critically important for us to redouble our efforts in assessing and implementing common user environments, practices, and tools within and across the centers. Your individual and collective user feedback through the User Advocacy Group makes it clear that you consider this to be one of your highest priorities for us.

In response, the HPCMP Office and the major centers within the program have formalized and chartered a Corporate Board of Directors (CBOD), tasked to develop policies and strategies in this regard—and to oversee the efforts of the many technical design, implementation, and maintenance teams who will contribute to this common environment.

My staff and I look forward to seeing you in June at the 2004 HPCMP Users' Conference in Williamsburg, Virginia. As always, please take every opportunity to let us know how we can better serve you—your feedback is critically important to us and to the HPCMP.

About the Cover:

Pictured are Navy Joint Strike Fighter (JSF) F-35B Jets, future generations of which will benefit from the research described in State-to-State Kinetics-Based Prediction of Thermal Nonequilibrium in Hypersonic Flows (Page 9) and Direct Numerical Simulation of Pulsed Jets in Cross-Flow (Page 14), as well as other projects underway at the NAVO MSRC.

The Naval Oceanographic Office (NAVO) Major Shared Resource Center (MSRC): Delivering Science to the Warfighter

The NAVO MSRC provides Department of Defense (DoD) scientists and engineers with high performance computing (HPC) resources, including leading edge computational systems, large-scale data storage and archiving, scientific visualization resources and training, and expertise in specific computational technology areas (CTAs). These CTAs include Computational Fluid Dynamics (CFD), Climate/Weather/Ocean Modeling and Simulation (CWO), Environmental Quality Modeling and Simulation (EQM), Computational Electromagnetics and Acoustics (CEA), and Signal/Image Processing (SIP).

NAVO MSRC
Code N7
1002 Balch Boulevard
Stennis Space Center, MS 39522
1-800-993-7677 or
msrchelp@navo.hpc.mil

NAVO MSRC Navigator
www.navo.hpc.mil/Navigator

NAVO MSRC Navigator is a biannual technical publication designed to inform users of the news, events, people, accomplishments, and activities of the Center. For a free subscription or to make address changes, contact NAVO MSRC at the above address.

EDITOR:
Gioia Furness Petro, petrogio@navo.hpc.mil

DESIGNERS:
Cynthia Millaudon, cynmill@navo.hpc.mil
Kerry Townson, ktownson@navo.hpc.mil
Lynn Yott, lynn@navo.hpc.mil

Contents

World's 10 Most Powerful Supercomputer Sites

1993 - 2003

Source: www.top500.org/lists/2003/11/TOP500_Nov03.pdf

Validation of the 1/8° Global Navy Coastal Ocean Model Nowcast/Forecast System

Charlie N. Barron, Lucy F. Smedstad, Robert C. Rhodes, A. Birol Kara, Clark Rowley, Richard A. Allard, and Harley E. Hurlburt, Naval Research Laboratory, Stennis Space Center, MS

One of the primary concerns driving the development of U.S. Navy global models is improved performance and nesting support in shelf and nearshore regions with short notice applicability anywhere on the globe. The global implementation of the Navy Coastal Ocean Model (NCOM) is a product of the effort at the Naval Research Laboratory (NRL) to meet this need.[1]

NCOM is the latest transition of the NRL first-generation global system, a progression of planned ocean analysis and forecast systems delivered for Navy operations at the Naval Oceanographic Office (NAVOCEANO).[2]

These systems include the Modular Ocean Data Assimilation System (MODAS)[3] and the 1/16° Navy Layered Ocean Model (NLOM).[4]

NLOM is a deep-water ocean model with higher horizontal resolution, soon to be increased to 1/32°, to better resolve mesoscale ocean dynamics.

The delivery of global NCOM provides a medium-resolution (1/8° or 14 kilometer (km) midlatitude) source for fully global upper-ocean prediction and boundary conditions for higher resolution coastal models.

Its 40 sigma-z levels are concentrated toward the surface to maintain a minimum rest thickness of 1 meter (m) in the uppermost layer.

In addition, NCOM provides a capability to be the ocean component for a global air-ocean forecast and embedded Arctic ice models. In joining the operational model suite at NAVOCEANO, NCOM extends prognostic model coverage to the entire global ocean, including coastal, Arctic, and Antarctic regions. Figure 1 illustrates the coverage in an Atlantic hemispheric view of assimilative NCOM 1998-2000 mean Sea Surface Temperature (SST). Together these model systems offer improved Navy operational global ocean analysis/prediction capability in coastal and open oceans.

The global NCOM system consists of the numerical model, associated databases, the assimilation system, and data extraction software. (Detailed descriptions of the NCOM controlling equations and numerical implementations are given in Barron et al.[5])

NCOM solutions are driven by atmospheric forcing from the Navy Operational Global Atmospheric Prediction System (NOGAPS) and assimilate temperature and salinity fields produced by MODAS using NLOM Sea Surface Height (SSH).

In addition, an NRL-compiled global database of monthly mean river discharge has been incorporated into NCOM, and model topography is based on a global, 2-minute gridded bottom topography produced at NRL.

Tides are not included in global NCOM but are optionally added by post-processing using the Oregon State University global tide constituent databases.[6]

Before transitioning global NCOM to operations, an evaluation of the system was necessary to quantify the accuracy of its products. The assessments provide measures of performance and model error that can be used to estimate product confidence and improve real-time assimilation. They also indicate a baseline for future upgrades to the global modeling system. A validated real-time, fully global ocean modeling system not only continually provides model nowcasts and forecasts wherever they are needed, but also affords a level of confidence in these products based on the verified level of performance in prior products.

Three interannual 1/8° global NCOM model simulations were integrated on 128 processors of the NAVO MSRC IBM SP3 (HABU): (1) free-running (i.e., atmospheric forcing only) 1998-2002, (2) assimilative (i.e., with ocean data assimilation of MODAS temperature and salinity fields) 1998-present, and (3) forecast mode 1998-2002 using restarts from the assimilative experiment.

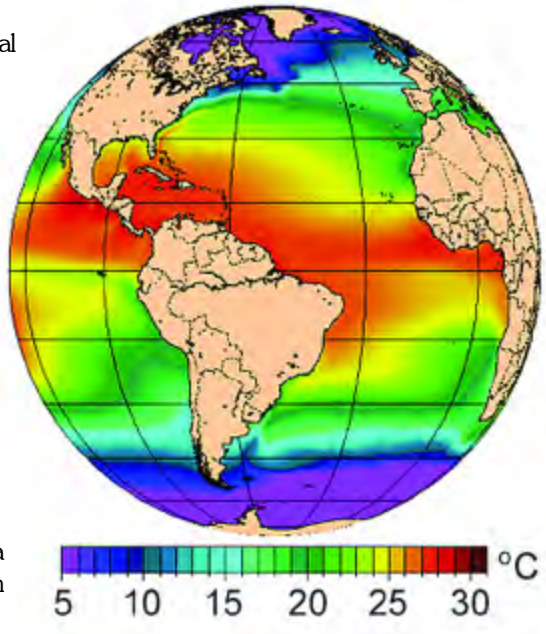

Figure 1. Assimilative 1/8° global NCOM 1998-2000 mean SST.

Continued Next Page...

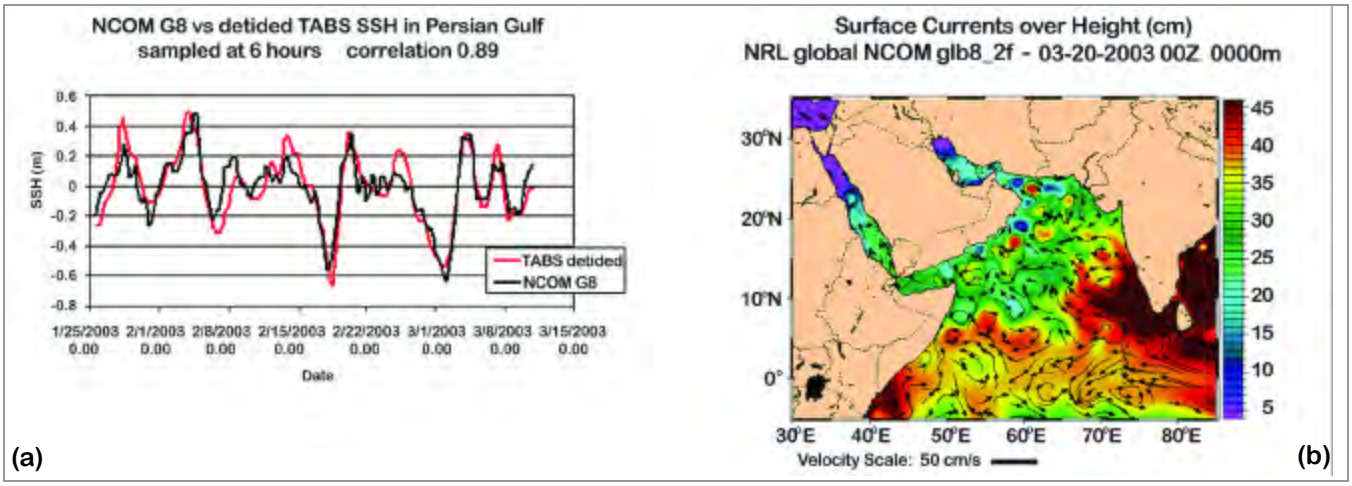

Figure 2. Assimilative 1/8° global NCOM SSH (a) compared with NAVOCEANO TABS buoy measurements 25 January - 15 March 2003 and (b) over the Arabian Sea on 20 March 2003.

The assimilative case corresponds to the operational implementation (although excluding in situ observations to allow independent validation), while the free-running case provides a reference for assessing stand-alone model skill and impact of assimilation.

All NCOM figures in this article are from the assimilative case. More information regarding global NCOM validations are reported by Kara et al.[7] and Barron et al.[8]

The validation test report[9] covers comparisons between unassimilated observations and a variety of NCOM results: temperature, transports, currents, kinetic energy, drifter trajectories, SSH, mixed-layer depth, and boundary conditions. The validations are broad and global but not exhaustive; more detailed examinations are possible for any aspect or region. An example of an SSH comparison is shown in Figure 2a.

Information for the model SSH is extracted at the location (not shown) of a NAVOCEANO observing buoy during the period before Operation Iraqi Freedom, and the two show good agreement. Results at this specific location combined with a validation of about 600 individual yearlong SSH time series around the world, showing a median correlation of .76, increase confidence in the accuracy of model SSH in other, non-corroborated locations, such as the broader Arabian Sea region in Figure 2b.

Means of observations offer another avenue for model evaluation. Eddy kinetic energy at 700 m from a 1998-2000 NCOM mean (see Figure 3a) shows similar patterns but lower energy than a mean of historical observations taken from Schmitz[10] (see Figure 3b).

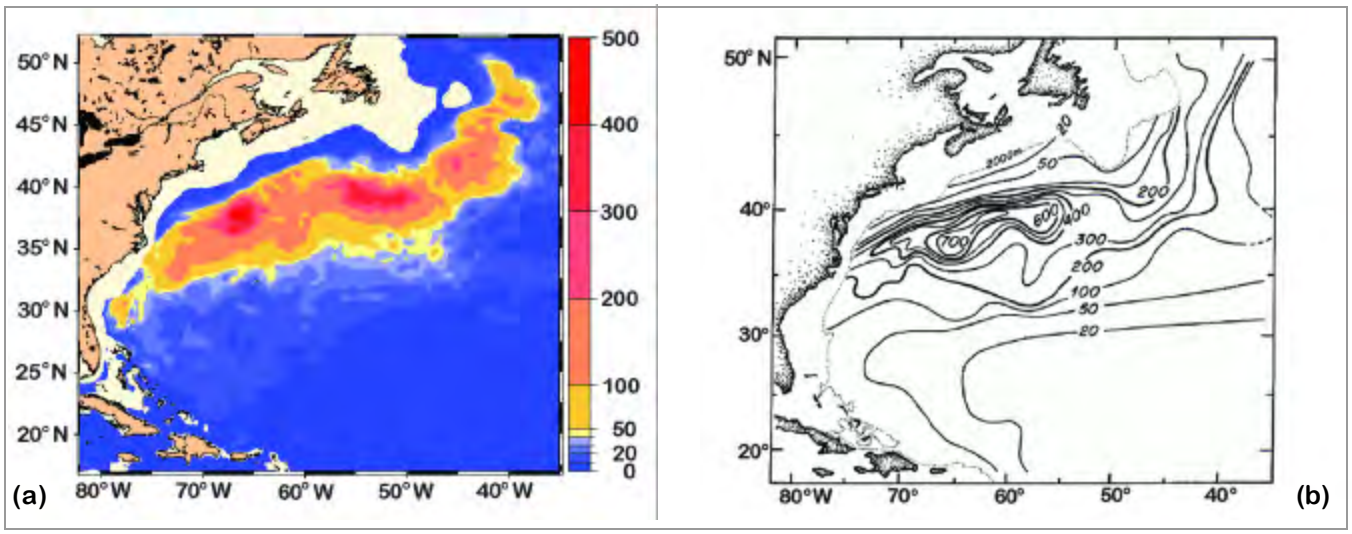

Figure 3. Eddy kinetic energy at 700 m from (a) the 1/8° global assimilative global NCOM 1998-2000 mean and (b) a mean of historical observations taken from Schmitz (1996).

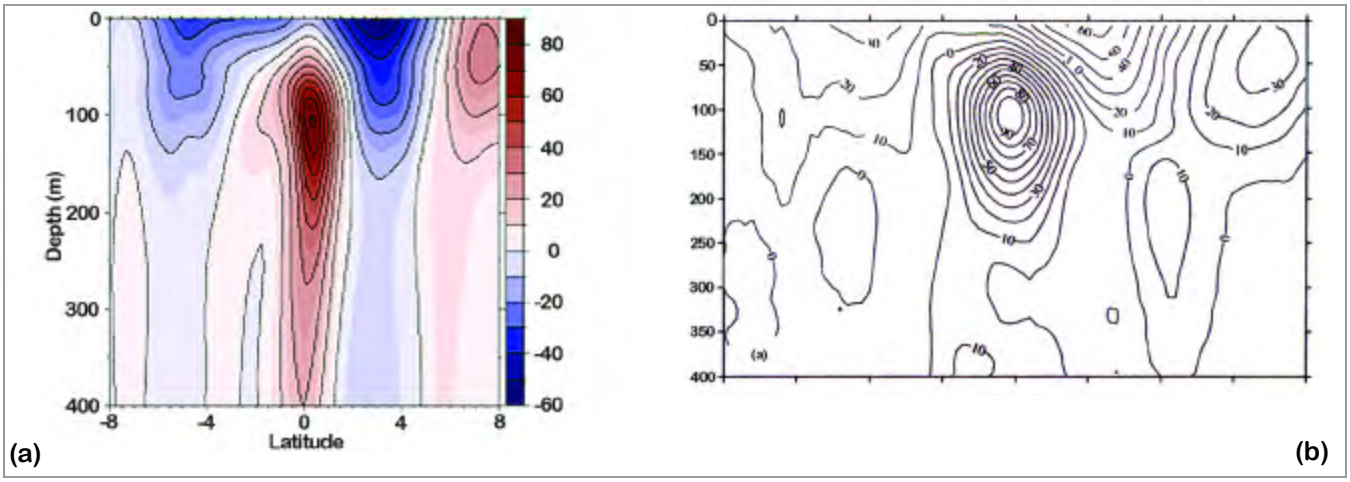

Figure 4. Equatorial cross section of eastward velocity at 135°W from (a) the assimilative 1/8° global NCOM 1998-2000 mean and (b) a 1991-1999 mean taken from Johnson et al.[11]

Despite different time spans, equatorial cross sections of velocity reflect good agreement between the 1998-2000 NCOM mean seen in Figure 4a and the mean calculated by Johnson et al.[11] for 1991-1999 (see Figure 4b), with the model yielding somewhat smaller peak speeds and showing vertical stretching at depth.

The resolution and model configuration for global NCOM is an attempt to best allocate resources for a timely, affordable, and useful system. Features and ocean processes on horizontal scales of 10 K or less cannot be represented by such a global model; these are instead relegated to nested models of smaller, regional domains with increasing resolution.

Figure 5 depicts some of these regional domains, including the East Asian Seas (EAS) NCOM and Intra-Americas Seas (IAS) that are in the transition pipeline. Global NCOM also supported nested relocatable models for Prestige oil spill clean-up activities off the coast of Spain in 2002-2003.

In addition, other areas and exercises have been supported, including activities in the Persian Gulf during Operation Iraqi Freedom.

Validation of the global NCOM system has shown the added value of the model transition. Areas for future improvements have also been identified. Presently the authors are continuing to improve the assimilation components by performing experiments with assimilation using the 1/32° NLOM, which is a planned upgrade, as soon as the NAVO MSRC expands to sufficient operational computing resources, likely late 2004. NCOM assimilation improvements will begin transition on a similar schedule, after completion of the NCOM operational testing.

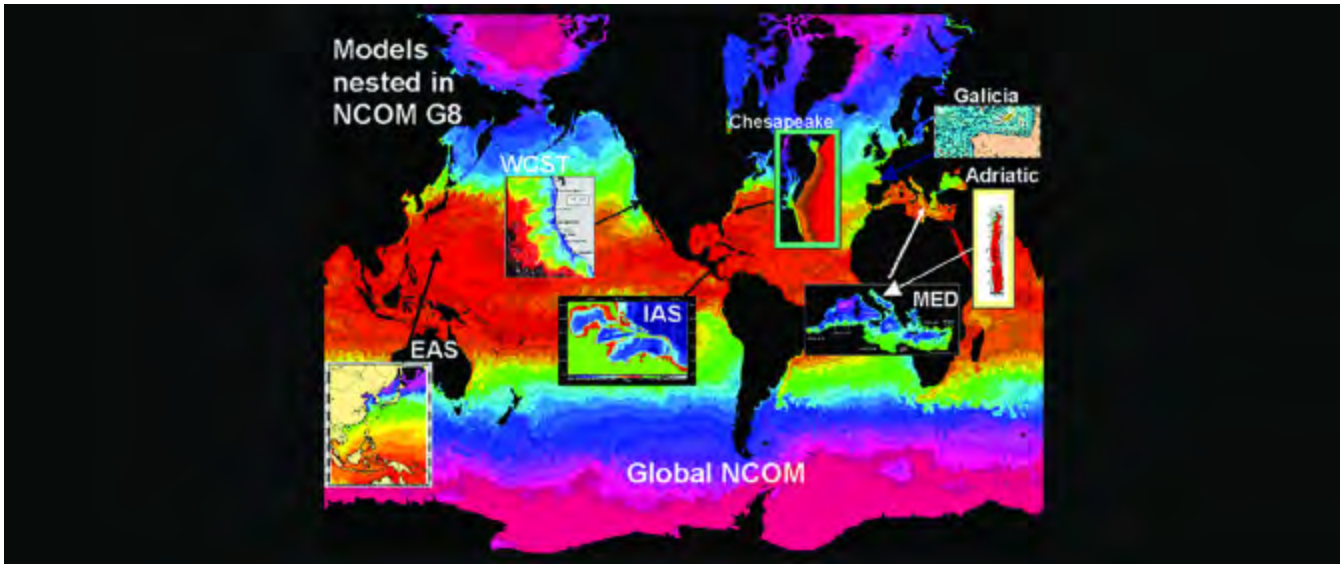

Figure 5. Snapshots from selected regional NCOM models that have been nested within global NCOM.

Acknowledgements

This work was funded as part of the NRL 6.4 Large-scale Models and 6.4 Ocean Data Assimilation projects, managed by the Commander, Space and Naval Warfare Systems Command (COMSPAWARSYSCOM) under program element 0603207N. The numerical simulations were performed on the NAVOCEANO IBM-SP3 (HABU) at Stennis Space Center, MS, using grants of computer time from the Department of Defense High Performance Computing Modernization Program (HPCMP). Additional development and parallelization of NCOM were supported by the HPCMP's Common High Performance Computing Software Support Initiative under projects CWO-01 and CWO-07, and under the High-Fidelity Simulation of Littoral Environments Portfolio. Special thanks go to D.S. Ko for the topography and model grid, Joe Metzger for data comparisons, and Jan Dastugue for help with graphics.

References

1. Barron, C.N., R.C. Rhodes, L.F. Smedstad, P.J. Martin, and A.B. Kara, 2003: "Global Ocean Nowcasts and Forecasts with the Navy Coastal Ocean Model (NCOM)," 2003 NRL Review, 175-178.
2. Rhodes, R.C., H.E. Hurlburt, A.J. Wallcraft, C.N. Barron, P.J. Martin, E.J. Metzger, J.F. Shriver, D.S. Ko, O.M. Smedstad, S.L. Cross, and A.B. Kara, 2002: "Navy Real-Time Global Modeling Systems," Oceanography, 15, 29-43.
3. Fox, D.N., W.J. Teague, C.N. Barron, M.R. Carnes, and C.M. Lee, 2002a: "The Modular Ocean Data Assimilation System (MODAS)," Journal of Atmospheric and Oceanic Technology, 19, 240-252.
4. Smedstad, O.M., H.E. Hurlburt, E.J. Metzger, R.C. Rhodes, J.F. Shriver, A.J. Wallcraft, and A.B. Kara, 2003: "An Operational Eddy-Resolving 1/16° Global Ocean Nowcast Forecast System," Journal of Marine Research, 40-41, 341-361.
5. Barron, C.N., P.J. Martin, A.B. Kara, R.C. Rhodes, and L.F. Smedstad, 2004b: "Global Navy Coastal Ocean Model (NCOM): Description and Application," Ocean Modeling, submitted.
6. Egbert, G. and L. Erofeeva, 2002: "Efficient Inverse Modeling of Barotropic Ocean Tides," Journal of Atmospheric and Oceanic Technology, 19, 183-204.
7. Kara, A.B., C.N. Barron, P.J. Martin, R.C. Rhodes, and L.F. Smedstad, 2004: "Global Navy Coastal Ocean Model (NCOM): Description and Validation of Interannual Simulations," Ocean Modeling, in review.
8. Barron, C.N., A.B. Kara, H.E. Hurlburt, C. Rowley, and L.F. Smedstad, 2004a: "Sea Surface Height Predictions From the Global Navy Coastal Ocean Model (NCOM) During 1998-2001," Journal of Atmospheric and Oceanic Technology, submitted.
9. Barron, C.N., A.B. Kara, R.C. Rhodes, C. Rowley, and L.F. Smedstad, 2004c: "Validation Test Report for the 1/8° Global Navy Coastal Ocean Model Nowcast/Forecast System," NRL Formal Report in preparation.
10. Schmitz, W.J., 1996, "On the World Ocean Circulation: Volume I. Some Global Features/North Atlantic Circulation," Woods Hole Oceanographic Institution Technology Report, WHOI-96-03, 150 pp.
11. Johnson, G.C., M.J. McPhaden, and E. Firing, 2001: "Equatorial Pacific Ocean Horizontal Velocity, Divergence, and Upwelling," Journal of Physical Oceanography, 31, 839-849.

State-to-State Kinetics-Based Prediction of Thermal Nonequilibrium in Hypersonic Flows

Eswar Josyula, Computational Sciences Center of Excellence, Air Force Research Laboratory, Wright Patterson Air Force Base

Sustained hypersonic flight and rapid, routine access to space pose daunting challenges associated with the harsh environment encountered by vehicles traveling at extremely high speeds. Figure 1 depicts two relevant examples of these challenges: the external flow around the X-15 aircraft and internal flow in a rocket engine.

To successfully meet these challenges, testing is required to evaluate advanced designs and technologies to be employed on the next generation of hypersonic vehicles. However, there are many difficulties in conducting ground and flight tests. The wide-ranging spatio-temporal scales that arise at high temperatures are one of the many difficulties that must be overcome in these tests.

The cost and difficulty of conducting ground and flight tests accentuate the need for complementary simulation techniques to reduce the number of tests. However, a mathematical simulation of the thermodynamic nonequilibrium processes of hypersonic flows is extremely difficult to develop. This article provides a brief overview of these challenges, develops a simulation framework, and applies this framework to hypersonic flows around a vehicle forebody and flows inside an expansion nozzle.

CHALLENGES

Accurate computations in the time scales of the kinetic processes in trans-atmospheric flowfields require knowledge of the reaction processes' finite rates. The proper simulation and understanding of these thermodynamic nonequilibrium processes occurring in the flowfields of the high speed systems are crucial for prediction of aeroheating and drag in external flows around vehicles and thrust in the internal flows of propulsive nozzles.

The proper treatment of energy transfers between nonequilibrium molecular energy modes and the dissociation and ionization processes has important implications in the accurate prediction of the aerodynamic heating on hypersonic vehicles and thrust in propulsive nozzles. In turn, nonequilibrium vibrational energy distributions are required for prediction of dissociation rates, interpretation of radiation experiments, and interpretation of ionic recombination rates.

At high temperatures, molecular collisions result in the exchange of the translational, rotational, vibrational, and electronic energies with the collision partners. The probabilities of these elementary processes differ significantly, giving rise to widely separate relaxation times for the internal modes. Thus, it becomes important to account for the rates of relaxation processes to predict the nonequilibrium behavior. Vibrational equilibration, in particular, involves widely separated relaxation times, ranging from the very short times for translational/rotational equilibration to the longer times for chemical and ionization equilibration. The disparate eigenvalues of these relaxation times have significant physical and computational implications.

Continued Next Page...

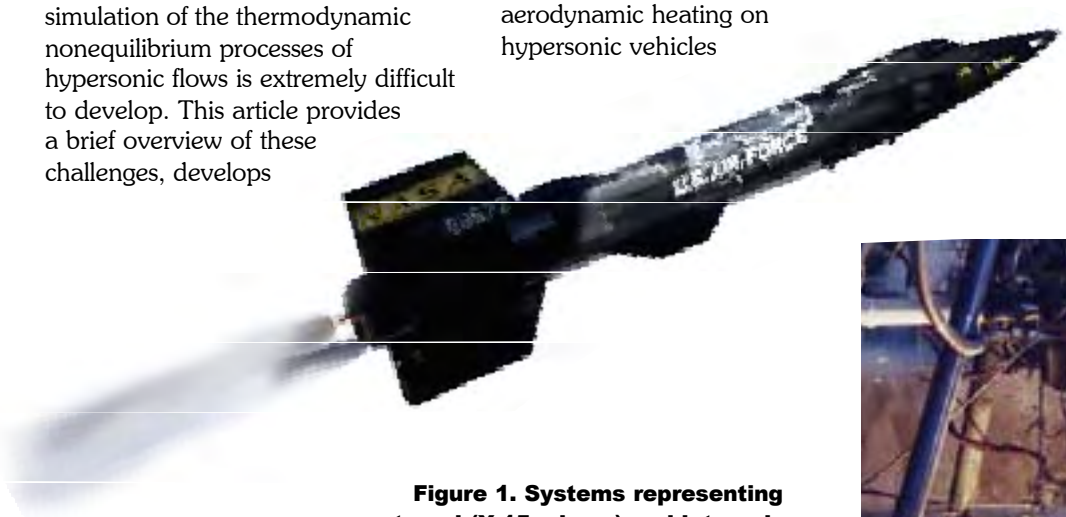

Figure 1. Systems representing external (X-15, above) and internal flows (Rocket nozzle, right) in thermal nonequilibrium (images taken from http://www.grc.nasa.gov/WWW/K-12/airplane/rocket.html).

METHODOLOGY

The most fundamental mathematical description of modeling the kinetic processes associated with the internal energy excitation of the vibrational and rotational modes is given by the master rate equations.

These time-dependent differential equations account for the population distributions in the quantum energy states by considering the kinetics of particle exchanges and can thus account for non-Boltzmann distributions that do not assume a mean energy for the vibrational modes.

Figure 2 shows a schematic of the potential energy well depicting the various kinetic processes of vibration-translation, vibration-vibration, and dissociation transfers that could occur as a result of vibrational energy excitation.

The master rate equations are coupled to macroscopic fluid dynamic equations to form a set of conservation equations: mass, momentum, and energy in the flowfield. The mass conservation equations, however, are written for each quantum level and thus give rise to a very large and mathematically complex set of partial differential equations.

The number of quantum levels depends on the energy of dissociation of the molecule. For example, the two principal constituents of air—nitrogen and oxygen—require 47 and 33 quantum levels respectively.

For a nitrogen-nitrogen collision, master rate equation calculations account for the energy exchange processes amongst the 47 quantum energy levels of the nitrogen molecule.

These calculations determine the probability of a specific process contributing to the dissociation process. As an example, the probability of vibration-vibration energy transfers in a nitrogen gas maintained at 5000° Kelvin (K) contributing to the dissociation process is depicted in Figure 3.

The axes in Figure 3, represented by i and j, denote the quantum levels in nitrogen molecule A colliding with nitrogen molecule B. As seen in the figure, the high energy exchange probability is primarily in the lower levels of the vibrational manifolds of both colliding molecules. The mathematical complexity of the non-linear governing partial differential equations requires concomitantly advanced numerical methods.

Consequently, the Roe flux-difference split method is employed to solve the coupled set of equations. The method is implemented in a finite volume formulation by computing the cell interface fluxes.

The mass conservation equation is written for mass density in each quantum level. The source term of production and destruction of "species" derived from the vibrational master equations is composed of the relevant energy exchange processes, consisting of the V-T and V-V reaction mechanisms.

SOLUTIONS

VIBRATIONAL NONEQUILIBRIUM

The distribution of computed vibrational levels for a Mach 6.5 nitrogen flow past a forebody is shown in Figure 4.

The plots show fractional density versus vibrational quantum level energies with the corresponding quantum numbers identified along the curves. Population distributions versus quantum level vibrational energies are plotted along four select locations along the stagnation streamline.

The four locations are Stream, Pre-Shock, Post Shock, and Stagnation Point (or Surface). The Stream location has freestream conditions and is several grid points before the onset of the bow shock; Pre-Shock (at the shock edge) is at the grid point immediately before the highest temperature and pressure values across the shock; and the Post-Shock location is the point immediately behind the shock-front in the shock layer. Figure 4 also shows that the population distribution is Boltzmann in the freestream and non-Boltzmann in the shock layer.

VIBRATIONAL EXCITATION LEADING TO DISSOCIATION

The study of the kinetics of thermal dissociation demonstrates that the dissociation process alters the vibrational distribution function. As equilibrium is approached, a quasi-steady state is achieved, and the populations obtain a self-similar form.

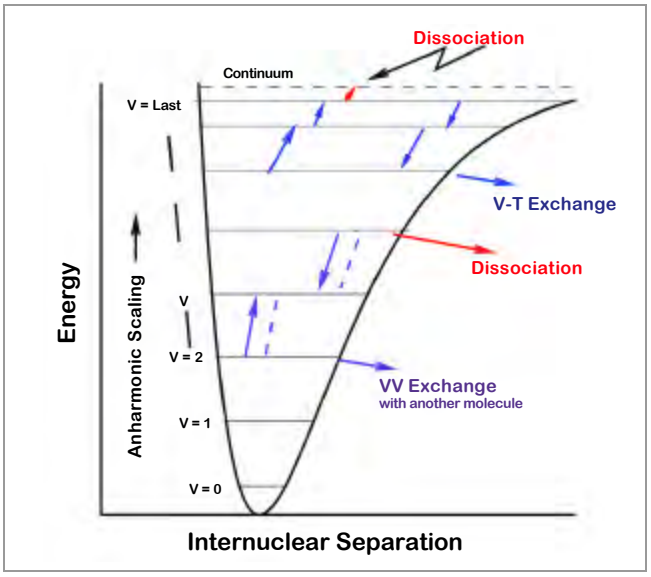

Figure 2. Energy transfers in the molecular vibrational manifold depicting energy exchange processes that occur over a wide range of time scales.

Figure 3. Probability of vibration-vibration energy transfers among the quantum states in nitrogen-nitrogen collision at 5000º K.

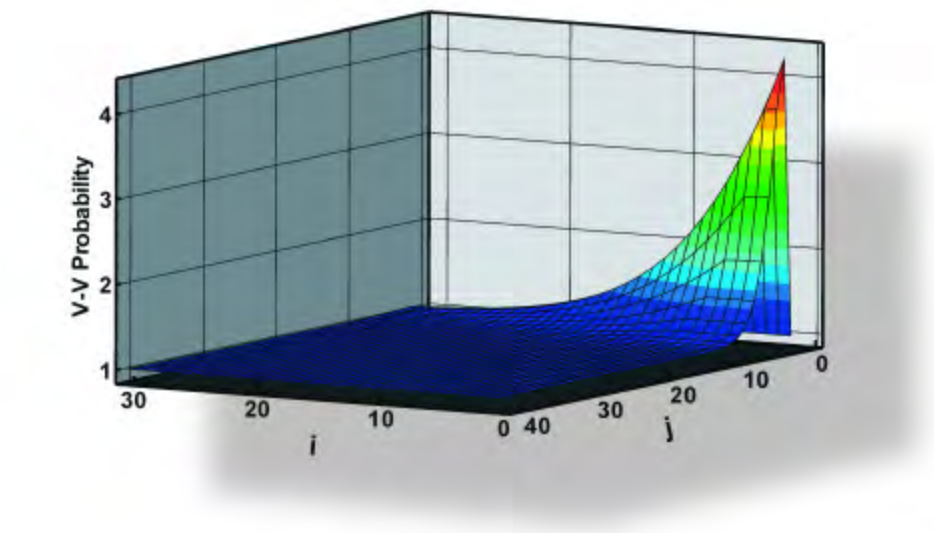

The dissociation losses from the vibrational manifold tend to reduce the vibrational populations below their equilibrium values, resulting in the lowering of the dissociation rate. At equilibrium, the net loss due to dissociation and recombination is zero, and there is no depletion of the population.

A state-to-state kinetic description of the nonequilibrium process allows the researcher to develop the internal energy mode coupling models, such as the vibration-dissociation coupling model, essential to the understanding of the aerothermodynamics of aerospace vehicles.

It is convenient to divide the vibrational relaxation into two time regimes. Initially, over a time t_{VT}, a quasi-steady distribution is established. Over a much longer time t_{diss}, this distribution approaches the equilibrium distribution, and the atoms and molecular species concentrations then ultimately satisfy the Law of Mass Action. Here, the evolution of the quasi-steady distribution as it evolves in time toward the equilibrium distribution is considered.

In the case of $t_{VT} = < t < t_{diss}$, two opposing factors characterize this state: V-T transfers seek to establish equilibrium, while dissociation disrupts and perturbs the distribution.

The nonequilibrium conditions behind the shock wave of the blunt body example discussed in Figure 4 exemplify the case where the translational temperature is greater than the vibrational temperature, ultimately approaching near-equilibrium conditions close to the surface of the body.

The higher rate of dissociation versus recombination in blunt body flows makes the vibrational population depletion effect significant in the vibration-dissociation coupling model. However, in expanding nozzle flows, which are critical for thrust development, the effect of vibration-dissociation coupling on the vibrational population density is reversed, and the population is enhanced.

For sonic flows at the inlet of an expansion nozzle, the flow is in thermal equilibrium, and as it proceeds towards the exit of the nozzle, the low departs from the equilibrium conditions. The vibrational temperature freezes near the inlet, the translation temperature rapidly falls as a result of the expansion process, and the flow exhibits higher degrees of nonequilibrium as it proceeds towards the exit. As the translational temperature starts dropping, the dissociation rate drops significantly.

However for the same translational temperature drop, the change in the recombination rate is small, and the recombination rate remains consistently higher than the dissociation rate throughout most of the nozzle flowfield.

Continued Next Page...

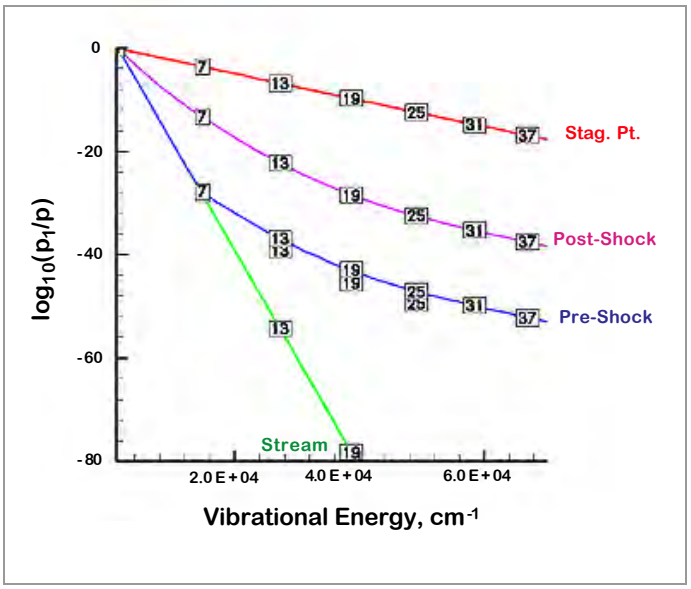

Figure 4. Nonequilibrium population distribution at select locations in a flow past a vehicle forebody, with Mach 6.5 nitrogen flow and a 1-meter forebody radius. The abscissa denotes the vibrational energy distribution in the quantum energy states of nitrogen.

This recombination-dominant flow leads to a population enhancement in the vibrational manifold under the nonequilibrium reactive conditions. A vibration-dissociation coupling model thus has to account for this enhancement to accurately predict the nonequilibrium chemistry. Figure 5 shows the population depletion and enhancement in high-speed flow situations.

The proper simulation and understanding of the thermodynamic nonequilibrium processes occurring in the flowfields of the high speed systems are crucial for prediction of aeroheating and drag in external flows around vehicles and thrust in the internal flows of propulsive nozzles.

These simulations require solving a mathematically complex set of non-linear governing partial differential equations. The solution of these sets is computationally intensive and requires the computational capacity provided by High Performance Computing architectures.

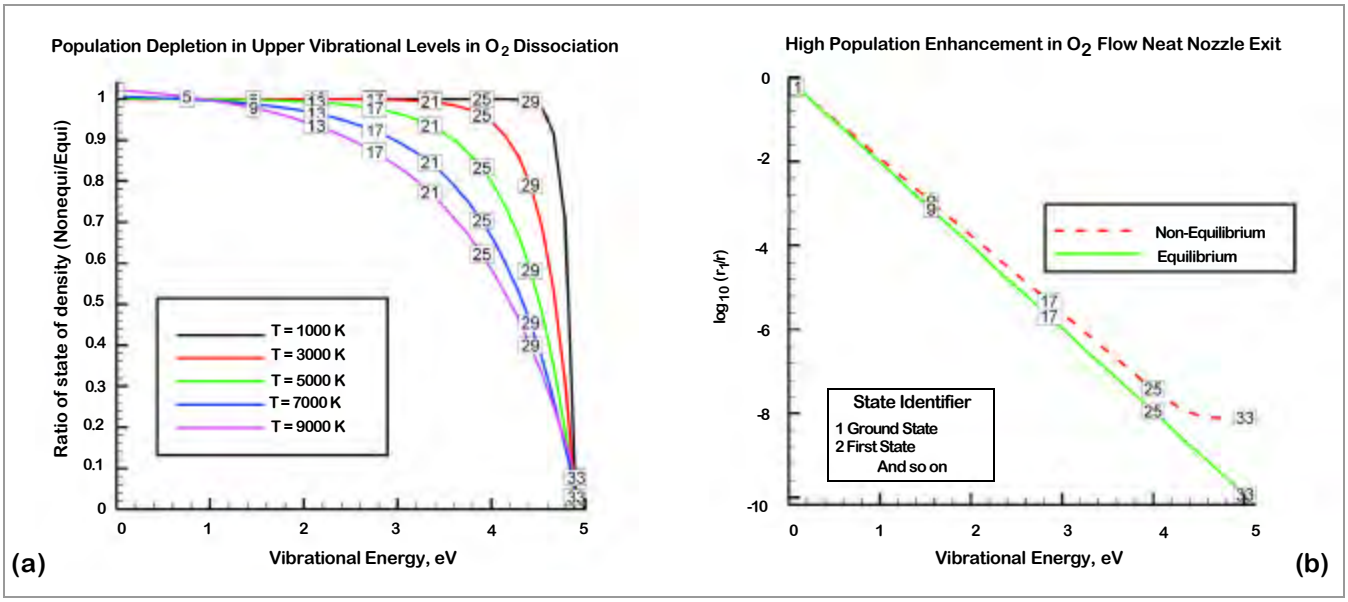

Figure 5. Vibrational population depletion and enhancement signifying departure from equilibrium conditions in high-speed flows, (a) flow past a vehicle forebody, (b) flow inside an expansion nozzle for equilibrium throat temperature of 5000° K and exit translational temperature of 2548° K and exit vibrational temperature of 2761° K.

Acknowledgements

This research was supported under U.S. Air Force Office of Scientific Research. Computer resources were provided by the U.S. Department of Defense, High Performance Computing, Major Shared Resource Center at the Naval Oceanographic Office, Stennis Space Center, MS.

References

1. Josyula, E., "Computational Study of Vibrationally Relaxing Gas Past Blunt Body in Hypersonic Flows," Journal of Thermophysics and Heat Transfers, 14, pp. 18-26, 2000.
2. Josyula, E. and W.F. Bailey, "Vibration-Dissociation Coupling Model for Hypersonic Blunt Body Flow," AIAA Journal, 41, 1611-1613, 2003.
3. Josyula, E. and W.F. Bailey, "Vibrational Population Enhancement in Nonequilibrium Hypersonic Nozzle Flows," 36th American Institute of Aeronautics and Astronautics Thermophysics Conference, Orlando, FL, June 23-26, 2003.
4. Shizgal, B.D. and F. Lordet, "Vibrational Nonequilibrium in a Supersonic Expansion with Reaction: Application to O2-O," Journal of Chemical Physics, 104, 3579-3597, 1996.
5. Osipov, A.I. and E.V. Stupochenko, "Kinetics of the Thermal Dissociation of Diatomic Molecules I. Small Impurity of Diatomic Molecules in a Monoatomic Inert Gas," Combustion, Explosion and Shock Waves, Translated from Fizika Goreniya i Vzryva, 10, 303-313, 1974.
6. Capitelli, M., C. Gorse, and G.D. Billing, "V-V Pumping Up in Nonequilibrium Nitrogen: Effects on the Dissociation Rate," Chemical Physics, 52, 299-304, 1980.

NAVO MSRC Visualization: Open Source Solutions

Sean Ziegeler, NAVO MSRC Visual Analysis and Data Interpretation Center (VADIC)

Open source and free software products are gaining significant popularity in business and government. Open source products have several advantages that compel organizations to consider them as viable alternatives to commercial software.

In most cases, the greatest advantages are that open source software is free—which can result in significant savings and is hardware platform independent—which enables users of open source software to select the most cost-effective hardware for their application.

In addition, applications developed using open source software can be redistributed without cost. So, in addition to having no cost to use, this results in another significant and attractive advantage: there will not be any licensing fees to distribute an application based on open source code.

At the NAVO MSRC Visual Analysis and Data Interpretation Center (VADIC), these aspects of open source tools have enabled the production of higher quality and more affordable products for VADIC clients. This article uses the example of the VADIC work for the National Aeronautics and Space Administration (NASA) Goddard Space Flight Center on Sea Surface Temperature (SST) images to demonstrate the open source advantages.

The Open Source Advantage

At the heart of the open source software phenomena is that small groups of enthusiasts can evolve into a worldwide collaborative effort. This, in turn, fosters tremendous growth in the software, which leads to innovation and, in the end, culminates in full-featured software that can compete with its commercial counterparts. One of the most convincing examples of this is Linux, which began as one person's hobby, and has become a practical, powerful operating system with hundreds of contributors and even more users around the world. Similarly, many organizations utilize the popular Apache software to manage their Web servers, and many information systems are implemented using MySQL, a popular database management tool. In fact, the tools range in complexity from entire compilers, such as GNU C++, to Web browsers like Mozilla.

Transitioning to open source products usually involves an evaluation period, when the legacy application and the new, open source-based application

Continued Page 25...

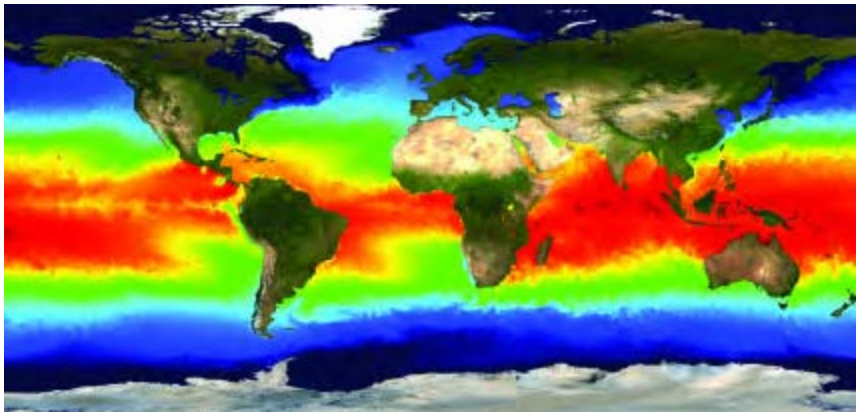

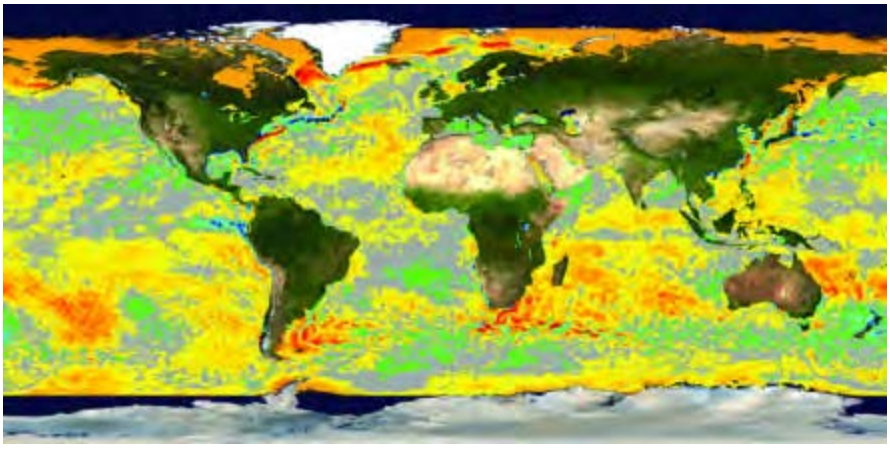

Figure 1. (Above) Sea Surface Temperature (SST), ranging from cold (blue) to warm (red).

Figure 2. (Left) SST Anomaly, ranging from below average (blue) to above average (red).

Direct Numerical Simulation of Pulsed Jets in Cross-Flow

Frank Muldoon, Louisiana State University

Jets of fluid issuing into a cross-flow of fluid jets in cross-flow occur in a number of different applications such as film cooling for turbine blades, thrust and noise control of Vertical Take Off and Landing (VTOL) aircraft, fuel-air mixing in gas turbine combustors, and pollutant dispersion from chimney stacks.

Experiments with non-reacting flows have shown that pulsing the jet can have a large effect on the mixing, spreading, and penetration of the free jet. Therefore, external modulation of the jet is a potential strategy for enhancement of the mixing effectiveness of jets in cross-flow. This improvement in fuel-air mixing leads to better overall performance in a variety of applications (e.g., combustion).

Direct Numerical Simulations and Tetra

The goal of the present study is to computationally analyze the effect of external modulation (pulsing) on the flow structures and the resulting mixing of a jet in cross-flow.

As the flow is inherently unsteady (due to the external pulsing), the key to the successful prediction of such flows is the ability to resolve the dynamics of all important flow structures that result from the interaction of the unsteady pulsed jet with the main flow in the combustor.

In addition, to understand why external excitation changes the flow, it is necessary to resolve and track the different dynamic

flow structures resulting from different external excitations.

As a result, time-averaged Reynolds Averaged Navier-Stokes solutions provide very little insight into the issues of interest in the present work. Therefore, a Direct Numerical Simulation (DNS) is performed, and the results are used to examine the effects of forcing on the flow structures and mixing. To aid in quantifying the mixing, an equation governing the evolution of a passive scalar is solved along with the incompressible Navier-Stokes equations.

Another reason for performing a DNS of this flow (as opposed to an experimental study) is that a computational study can provide information that is very difficult to obtain in an experimental study. In the present work, massless particles are released into the flow at various locations.

These particles are colored by their seed locations and residence time, greatly aiding the understanding of the dynamics of the flow. Unlike in experiments, these particles can be introduced at arbitrary locations without the detrimental effect of the presence of physical seeding apparatus influencing the flow.

In this work, a single jet in a cross-flow is studied. The Reynolds number based on Ujet and jet diameter (d) is 5000,

Continued Next Page

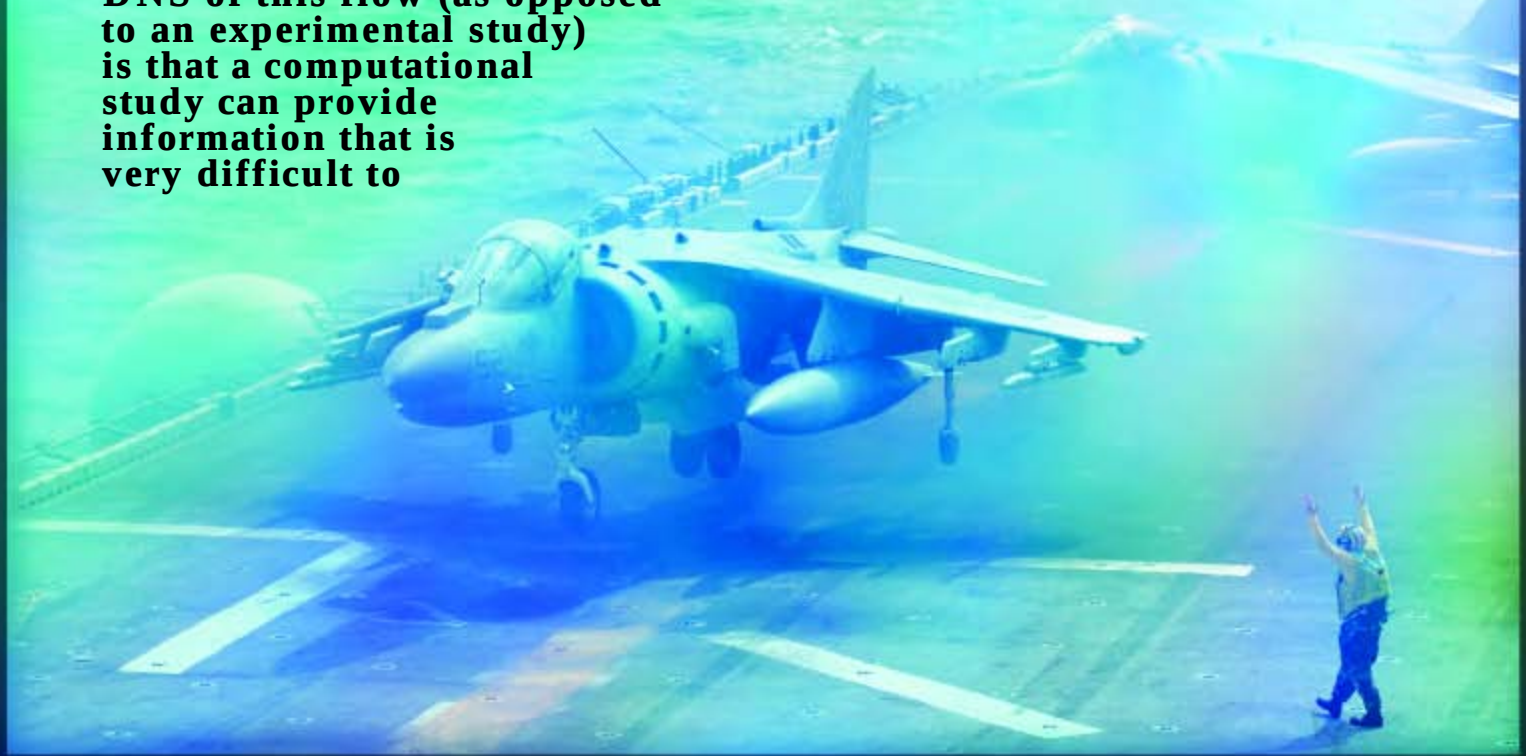

while the blowing ratio, defined as U_{jet} divided by the maximum cross-flow inlet velocity, is 6. The jet is injected at 90 degrees to the cross-flow. The scalar at the jet exit is set to one, while at the cross-flow inlet, it is set to zero. Referring to Figure 1, L_y=17d, L_p=10d, L_{up}=7d, and L_{down}=25d. Solutions are obtained on three different grids that contain 2, 15, and 120 million grid points. The time step used results in maximum Courant-Friedrich-Levy (CFL) numbers of approximately .3 at any point in the domain.

After reaching a statistically steady state, turbulent statistics are collected at each time step until the flow (based on the cross-flow velocity) has traveled a distance equal to 534 jet diameters (d). As statistics are collected at every time step, this results in statistics being averaged over 160,201 distinct realizations of the flow field.

Solutions to this flow problem are obtained by the use of the Tetra[1] computer program developed by Frank Muldoon at Louisiana State University (LSU).

Tetra solves the incompressible Navier-Stokes equations as well as equations governing the transport of passive scalars. It can also efficiently track numerous massless particles (up to 20 million have been used in these simulations).

In Tetra, a spatially sixth-order accurate central difference scheme with a monotonic limiter is used for the convective terms, while a fourth-order accurate central difference scheme is used for the diffusive terms. The convective and diffusive terms are integrated in time, using an explicit third-order accurate method, while the colored Symmetrically Coupled Gauss-Seidel method is used to solve the Navier-Stokes equations.

Tetra is written in FORTRAN 95 and parallelized using the Message Passing Interface (MPI). Tetra has been run on parallel machines such as the CRAY T3E, SGI Origin 3000, Helix (Linux cluster at LSU), and an IBM SP4 (MARCELLUS) at the NAVO MSRC.

The simulations in this article were run on MARCELLUS using 8 to 16 processors for the 15 million and 128 processors for the 120 million grid point grids. Based on wall clock time, the 120-million grid point simulation attains 2.5×10^{-8} seconds per time step per grid point.

Strouhal Numbers and Waveforms

The forcing frequency can be characterized by a dimensionless jet Strouhal number (kd/Ujet), where k is the forcing frequency in Hertz (Hz). In the present work, the modulation amplitude is such that the instantaneous mass flow through

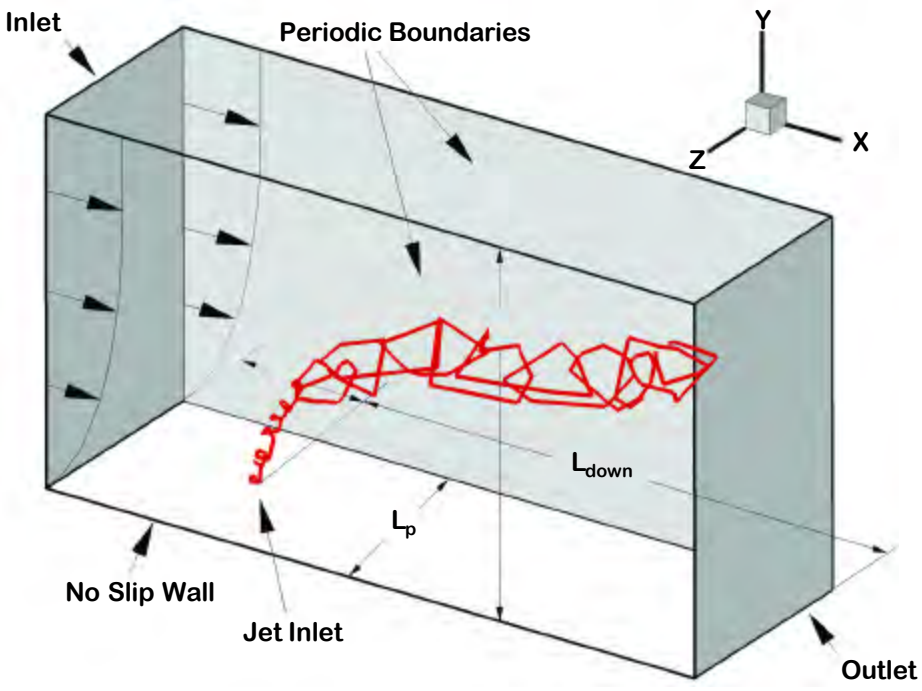

Figure 1. Problem schematic.

the jet exit is always between 80 and 120 percent of the time-averaged mean mass flow through the jet exit.

In the course of this work, a range of Strouhal numbers (.025, .05, .1, .2, .4, .6, .8, and 1) were examined for sine, square, and spiked waveforms on the coarsest grid. This was done to inexpensively identify combinations of Strouhal numbers and waveforms for which there are significant changes in the flow.

As dramatic changes in the mixing, spreading, and penetration of the jet were observed at Strouhal numbers of .2, .4, and .6 for the sine wave forms, a DNS is performed for these cases along with the unpulsed case.

In this study, pulsing at a Strouhal number of .4 causes the jet to split into three vertical jets and to penetrate much further, while a Strouhal number of .6 causes the jet to split into two horizontal jets and to remain much closer to the jet exit (see Figure 2). Pulsing at a Strouhal number of .2, however, causes the jet to split into two vertical jets.

In addition, it has been found that the merging of the shear layer vortices at the leading edge of the jet occurs at Strouhal numbers of .2 (see Figure 3) and .6.

At a Strouhal number of .6, this merging occurs at approximately the same location that the jet bifurcates in the horizontal direction and is likely related to the bifurcation. For pulsed cases the frequency of the shear layer vortices which form at the front of the jet is that of the imposed pulsing, while for the unpulsed case the frequency of the shear layer vortices corresponds to a Strouhal number of .35.

Wake Vortices

While it is commonly thought that the wake vortices originate in the incoming wall boundary layer, the results of this work show a different origin for the wake vortices. Based on particle traces, it can be ascertained that the wake vortices do not contain any jet fluid.

The core of the wake vortices has its origin in fluid (i.e., green particles) at the back of the jet close to the wall (see Figure 4). This fluid is entrained into the shear layer vortices at the back of the jet. Part of this fluid, at the very back of the jet, is stripped off by the cross-flow and forms the seed or core of the wake vortex.

As the wake vortex moves downstream, it grows in diameter as cross-flow fluid (yellow particles),

Article Continues Next Page

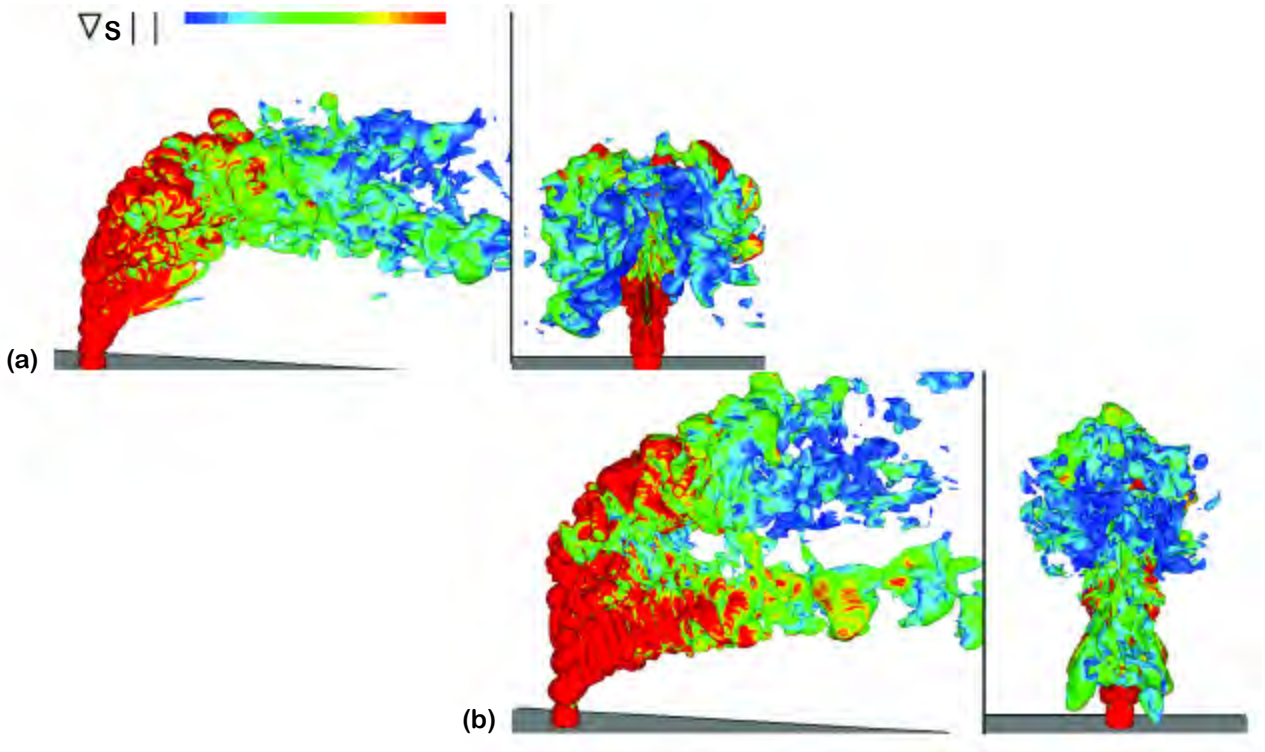

Figure 2. 0.1 Iso-surfaces of scalar colored by magnitude of gradient of scalar (a) Strouhal =.6, (b) Strouhal = .4.

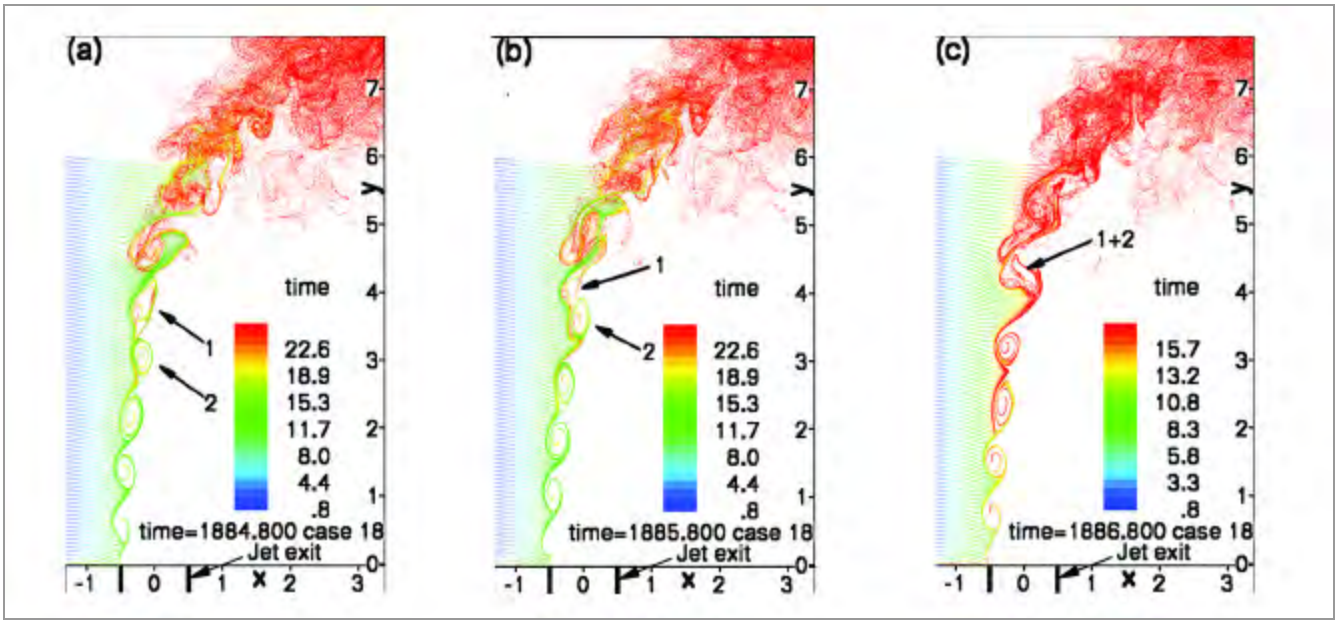

Figure 3. Shear layer vortex merging at Strouhal =.6, particles colored by residence time.

originating upstream of the jet, wraps around the seed or core of the vortex.

As the wake vortices move downstream, they feed fluid from the cross-flow into the jet. The center of the vortices continues to be dominated by fluid originating at the back of the jet close to the wall. This fluid travels along the center of the wake vortices in a corkscrew fashion upward into the jet. It is surrounded by fluid originating upstream of the jet, which also travels in a corkscrew fashion upward into the jet, representing a mechanism by which the jet is diluted by the surrounding flow. Pulsing at a Strouhal number of .6 completely suppresses the wake vortices.

Symmetry and Asymmetry in Flow Models

Though it is often assumed that symmetry will exist in the time-averaged results, this may not be the case. Asymmetry in the cross-stream plane has been found in a few experimental works but has not been extensively studied.

While it is impossible in an experiment to remove all asymmetries regarding elements such as the incoming flow, the physical geometry of the jet nozzle, etc., much greater control exists in computations.

In the present work, there are two sources of asymmetry: round-off error and symmetry breaking in the initial conditions (used to hasten transition to turbulence).

The round-off error is a source of asymmetry because, while the same numbers are in a finite difference stencil on both sides of the z-axis, the numbers are added together in a

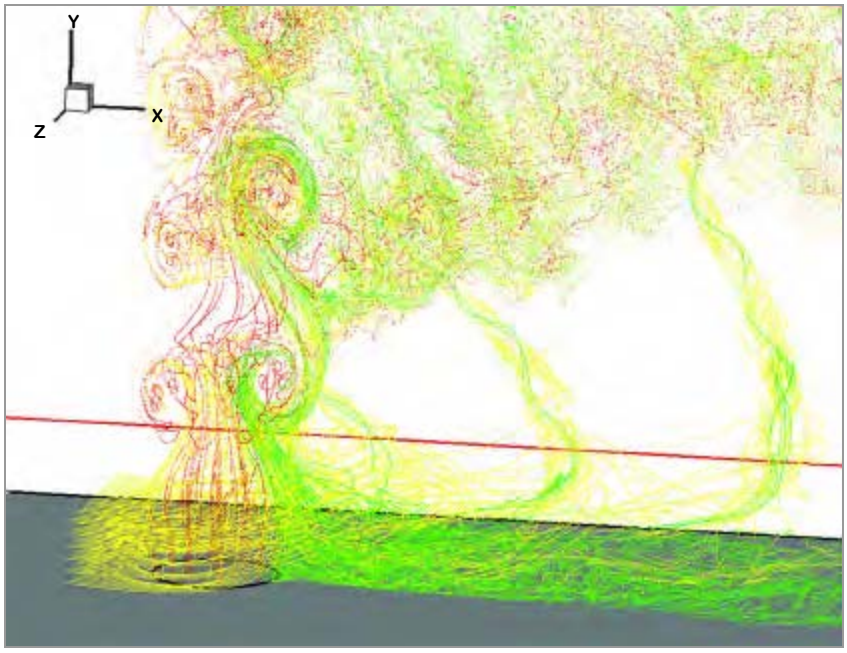

Figure 4. Wake vortex formation, at Strouhal number of .4.

different order on each side of the z-axis. No asymmetry is introduced by the boundary conditions, as they are symmetrical about the z-axis.

The asymmetry caused by the round-off error is very small, while the asymmetry resulting from the initial conditions should decay (in a time-averaged sense) if physically an asymmetry does not exist. In the present work, asymmetry exists only for the unpulsed jet and for sine wave pulsing at a Strouhal number of .2.

Figure 5a shows the results of symmetry breaking in the initial conditions, while Figure 5b shows the result of symmetric initial conditions. It can be seen that the flow can assume either of these two apparently mirror image states.

Therefore, it can be concluded that for cases in which asymmetry is seen, the flow is very susceptible to asymmetries and that one of the two asymmetric states would appear in an experiment in which asymmetries in the initial and boundary conditions would likely be larger than the computations.

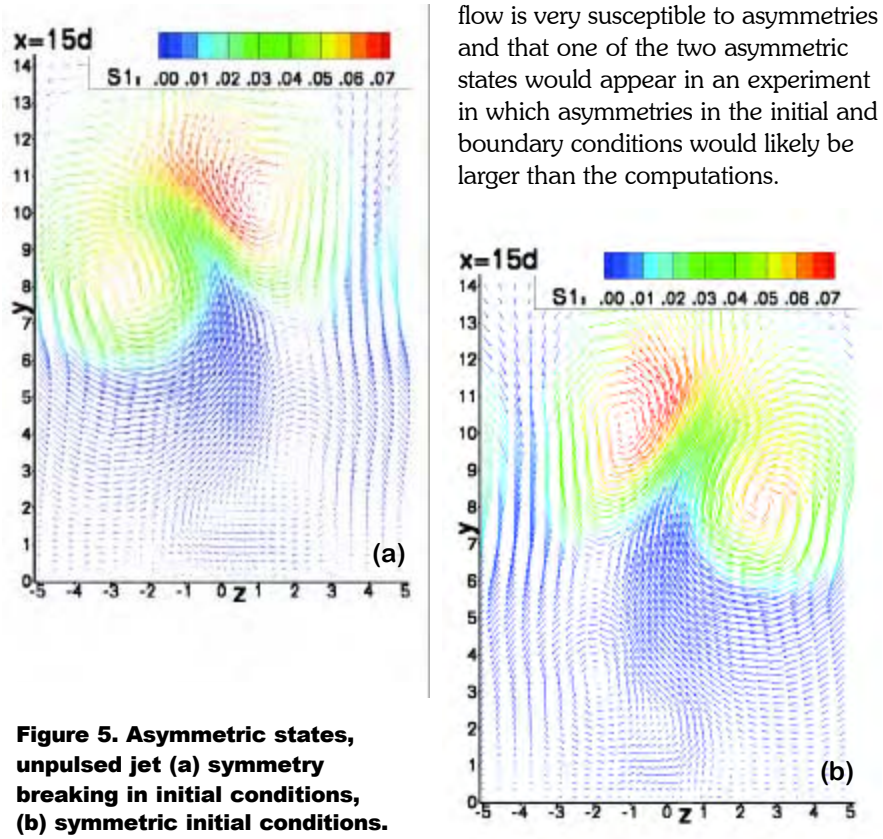

Figure 5. Asymmetric states, unpulsed jet (a) symmetry breaking in initial conditions, (b) symmetric initial conditions.

Conclusion

In conclusion, by analyzing the results of a DNS, a new origin has been found for the formation of wake vortices, while at certain pulsing frequencies the wake vortices can be suppressed. Also, a significant asymmetry that primarily affects the wake vortices has been found for certain cases.

The finding of this asymmetry, which can occur in one of two mirror images, confirms that found in the experimental works of Narayanan, Barooah et al.[2] and Smith and Mungal.[3]

In the future, work on this question may include the storage of complete time sequences of data, enabling interactive seeding and tracking of particles.

One question that this investigation will help answer is whether the branches of the split jet (resulting from pulsing) preferentially contain fluid exiting the jet from certain regions of the pulsing wave. Also under consideration is the coupling of an optimization algorithm to Tetra to enable a more rational approach to determine types of pulsing resulting in improved mixing and/or penetration.

Acknowledgements

This work received support from the Office of Naval Research (Propulsion Program, Dr. Gabriel Roy, program officer). Visualizations of the data, using the visualization software Tecplot™, were done at the Visual Analysis and Data Interpretation Center (VADIC) at the NAVO MSRC and at the Scientific Visualization Laboratory at Aeronautical Systems Center (ASC) of the Wright Patterson Air Force Base MSRC. The work summarizes a chapter of the dissertation of Frank Muldoon, advised by Professor Sumanta Acharya, for a doctorate in Mechanical Engineering at Louisiana State University.

References

1. Muldoon, F., "Numerical Methods for the Unsteady Incompressible Navier-Stokes Equations and Their Application to the Direct Numerical Simulation of Turbulent Flows," Ph.D. thesis, Louisiana State University, 2004.
2. Narayanan, S., P. Barooah, et al., "The Dynamics and Control of an Isolated Jet in Cross Flow," AIAA Journal, 2003.
3. Smith, S. H. and M.G. Mungal, "Mixing, Structure, and Scaling of the Jet in Crossflow," Journal of Fluid Mechanics 357: 83-122, 1998.

THE PORTHOLE

(Left)
Louisiana and Mississippi Federal and State government officials tour the NAVO MSRC Remote Storage Facility (RSF). Steve Adamec, NAVO MSRC Director, explains the RSF's capability to support our Nation's future supercomputing requirements. In attendance were Gov. Kathleen Blanco, LA; Gov. Haley Barbour, MS; U.S. Senator Thad Cochran; U.S. Congressman Gene Taylor; Sean O'Keefe, NASA Administrator.

(Left) Bobby Knesel, NAVO MSRC Deputy Director; Ed Gough, Commander, Naval Meteorology and Oceanography Command, Technical/Deputy Director; Kim Curry, Chief of Naval Operations Technical/Deputy Director; Ed Johnson, NAVOCEANO Technical Director; and Mr. Bob Winokur, the new Chief of Naval Operations Technical Director.

(Right)
Bobby Knesel and Steve Adamec, NAVO MSRC, escort IBM VIPs through the NAVO MSRC.

(Right)
Steve Adamec, NAVO MSRC Director; Lt. Gen. James Clapper, Jr., USAF (Ret.), Director, National Geospacial-Intelligence Agency; and CAPT Phil Renaud, NAVOCEANO.

(Above) CAPT Phil Renaud, NAVOCEANO; Gen. Charles A. Horner, USAF (Ret.); Steve Adamec, NAVO MSRC Director.

(Left)
David Griffin, U.S. Special Operations Command; David Pitcher, MITRE Corp.; Dave Cole, NAVO MSRC.

(Right)
Dave Cole, NAVO MSRC, CAPT Vic Addison, Director, Programs and Requirements Division, CNO.

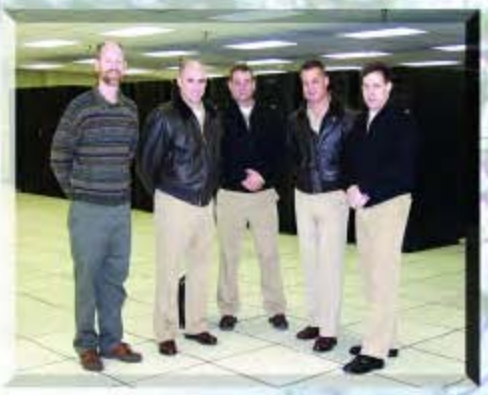

(Left)
Antisubmarine warfare helicopter pilots visit to learn about NAVO MSRC capabilities to support their mission.

(Right)
Executives of the National Geospacial-Intelligence Agency, escorted by Dave Cole, NAVO MSRC.

(Above) CAPT Rob Lawson, Deputy Oceanographer of the Navy; RADM Steven J. Tomaszeski, Oceanographer of the Navy; Steve Adamec, NAVO MSRC Director; CAPT Phil Renaud, NAVOCEANO.

(Right)
NGA representatives; Dr. Elizabeth Macaulay, Boeing; Dave Cole, NAVO MSRC; Patrick Hannon, NGA; Luanna Illing, Ball Aerospace; Susan MacLaughlin, NAVOCEANO.

(Above) Coahoma Community College students.

(Above) Jay Shriver, Naval Research Laboratory, provides an overview of the NRL projects run on NAVO MSRC resources to the Lockheed Martin Space Operations NAVO MSRC staff.

(Below, right, and far right)
The newly acquired Meteorology and Oceanography (METOC) Junior Officers tour the NAVO MSRC and the MSRC Visual Analysis and Data Interpretation Center (VADIC).

NAVO MSRC PET Update

Eleanor Schroeder, NAVO MSRC Programming Environment and Training Program (PET) Government Lead

This marks the beginning of the first option year of the PET contract. Hopefully most of you who have interests that fall within PET's scope have accounts on the Online Knowledge Center (OKC). The pages on that Web site underwent changes during the third contract year, and hopefully you have discovered that information is easier to find now. Of course, if you still have suggestions for improvement, we are always happy to hear them.

Year three did introduce some other changes as well. We brought on two additional people to augment core support for the Computational Environments (CE) functional area (FA). We did this to ensure a smooth transition of the Consistent Well-documented Computational Environment project into the core support arena. So I'd like to welcome both Brett Ellis and Joseph Thomas, both located at the University of Tennessee in Knoxville, to PET.

In the world of Climate, Weather, and Oceanography (CWO), we had difficulty finding a good candidate to fill the vacant onsite position at Engineer Research and Development Center (ERDC). As a result, we opted to do a temporary fix and are allowing the University of Texas, Austin, to hire a person to be a "roving onsite" for the next six months until we can find a permanent replacement to be located at a DoD installation. Of course, we still have our two extremely capable onsites, Dr. Tim Campbell at Stennis Space Center, MS, and Dr. John Romo in Monterey, CA.

Projects are still an integral of the PET program for this first option year of the contract. Project selections have been made, and detailed information can be found on the OKC.

In PET Component 1, we are continuing the support we have been providing to the Weather Research and Forecast (WRF) model, expanding the effort to integrate WRF into the Advanced Climate Modeling and Environmental Simulations Program (ACMES) based at the Air Force Combat Climatology Center (AFCCC). This should greatly benefit the AFCCC's operational effectiveness as well as benefit the many customers who utilize ACMES data in DoD operational activities.

The University of Hawaii, a Minority Serving Institution (MSI), was also awarded a project involving tropical cyclone forecasting. Planned enhancements to the Naval Operational Global Atmospheric Prediction System (NOGAPS) should improve the current NOGAPS tropical cyclone forecast skill.

We are looking at providing improved linear and nonlinear solvers for environmental quality modeling (EQM) codes. The expected outcome of this effort will be a set of semi-generic scalable, parallel solver modules that have been well-documented to allow the DoD users in EQM and similar areas to easily implement these solvers into their codes, thus improving the efficiency of the codes' compute times.

CE, PET Component 1's cross-cutting FA, is looking at four different issues. Two will be providing support to benchmarking/profiling of application data. One project is looking at automated collection of performance data into a database framework that will also offer a Java-based Application Program(ming) Interface (API) for performance analysis tools. The second effort will deploy and document a set of end-user tools for statistical analysis of large-scale performance data.

The Scalability and Performance Optimization Team (SPOT), an effort started in the third contract year that is similar to the Tiger Teams from the first PET program, will continue their work into this first option year. DoD users who have codes that they believe would benefit from this type of effort are encouraged to contact the SPOT members, myself, and/or their Computational Technology Area (CTA) lead to get assistance.

CE will also be delving into the area of dynamic process and fault-tolerance support for MPI-based varying load DoD applications. Concentration will be primarily on Signal and Image Processing applications this year, but we hope that the results will be extensible to other interested applications.

We have our work cut out for us this year, but PET Component 1 has an extremely well-qualified and enthusiastic group of partners that will perform this work. As their technical advisor, I am always open to hearing suggestions from you, our user community and customer base, for what we can do to further improve PET to better meet your needs.

User Data Storage Management

Sheila Carbonette, NAVO MSRC User Support

In the last few months, the total data archived on the Mass Storage Servers, JULES and VINCENT, have increased to over 900 Terabytes (TB).

The total number of archived user directories and files is in the millions and growing rapidly. Maintaining superfluous files or creating an overly complex directory structure will unnecessarily degrade performance. Therefore, we, the user community, should remove unnecessary files and streamline our directory structure. By practicing prudent storage practices, we can improve the overall performance of the storage management system.

During the last quarter, MSRC User Support sent a notice announcing the availability of monthly data summary reports to help users manage their archived data. Each monthly report will be stored as an ASCII file named **mas_store_usage** in each user home directory on the Archive Server. The **mas_store_usage** file for each user will be updated on the first day of each month. For example:

```
{jules:/u/home/shecar}[1]% ls -l
mas_store_usage-

rw-r--r--    1 shecar    other  166637 Mar
1 00:16 mas_store_usage
```

Each directory and subdirectory under your login account are listed in this report, with the number of files and data storage used per directory broken out by access age. The example below, lists the first line of the summary report file for user **shecar**:

```
jules:/u/home/shecar}[2]% head -1
mas_store_usage

shecar 64f 154.007GB (A/M: <1y) 57f
120.007GB (A/M: 1y-<2y)

6f 0.000GB (A/M: 2y-<5y) 1f 34.000GB
```

The directory **shecar** contains a total of 64 files that consume 154 Gigabyte (GB) of space. Of these 64 files, 57 files are less than one year old and take up 120 GB of space. There are six files that are between one and two years old taking up less than 1 GB of space. Lastly there is one file, taking up 34 GB of space, that has not been accessed in more than two years.

You can also determine the total amount of storage that you have used with the SAM/FS command **sdu**. This command, located in the /opt/SUNWsamfs/bin directory, is the SAM equivalent of the UNIX **du** command.

However, the **sdu** command includes both disk and tape storage media. For example:

```
jules:/u/home/shecar}[3]% sdu -sk .

1782983

ules:/u/home/shecar}[4]% du -sk .

157508  .
```

In addition, User Support will contact users whose data holdings on the Archive Servers exceed 1 TB and/or 100,000 files. This communication will request users to determine if nonessential files and directories can be deleted or consolidated. Again, a reduction in storage use or a consolidation of the directory structure will result in a performance improvement by saving archival server storage space and filesystem inodes.

The NAVO User Support group recognizes that data are critical to the users of the NAVO MSRC. Without data, there are no solutions to the problems being researched on the MSRC resources. In fact, without data there is no need for HPC resources.

We also understand that as the performance and capabilities of the HPC resources grow, the complexity of the problems solved on these resources also grows, which drives a corresponding growth in the data required and generated by solving these complex problems. Our interest is to ensure that we are using our data storage capacity efficiently and wisely. With an emphasis on optimal file management of their archived data, all NAVO users will benefit from a streamlined server storage structure with decreased overall system resource requirements.

If there are any questions or suggested improvements for the summary reports, please contact the NAVO MSRC User Support at 1-800-993-7677 or via E-mail to msrchelp@navo.hpc.mil.

NAVO MSRC Help Desk FAQs

Changing Kerberos Passwords

NAVO MSRC User Support

During the last quarter, NAVO MSRC implemented password aging on Kerberos passwords for all users homed at the NAVO MSRC. Users are now required to change their passwords every 90 days. The passwords created should be unique and secure and must be at least eight characters and contain three of the following characteristics: upper-case letters, lower-case letters, and numbers/special characters.

Users who create Kerberos tickets on a daily basis with *kinit* or through the *krb5.exe* application will receive a message that their password is about to expire. These expiration messages will begin within three weeks of the actual password expiration date and will continue until the password actually expires. This message will be displayed every time a user creates an initial Kerberos ticket.

Users who use only the Information Environment (IE) will not receive this expiration message. Until a solution is implemented, User Support will notify these users of their password expiration date and offer any assistance in changing their passwords. Below are instructions for changing passwords on a UNIX platform as well as a PC.

Changing Passwords on UNIX or LINUX Platforms

To change your Kerberos password on a workstation running the UNIX or LINUX Operating System, you must execute the **kpasswd** command as shown below.

```
{saturn:/u/home/shecar} [1]% Kpasswd shecar

Password for shecar@NAVO.HPC.MIL:
<ENTER OLD PASSWORD>

SAM Authentication

Challenge for Security Dynamics Mechanism

SecureID Passcode: <ENTER GENERATED
PASSCODE>

Enter new password: <ENTER NEW
PASSWORD.

Enter it again: <ENTER NEW PASSWORD
AGAIN>

Password changed.
```

Changing Passwords on the Windows Operating System

To change your Kerberos password on a workstation running the Windows Operating System, you must first execute the *krb5.exe* application. Once the *krb5.exe* application is running, select the **Change Password** button at the bottom of the dialog box.

A dialog box will appear prompting you to enter your **Name**, **Realm**, **Old Password**, and **New Password** twice. After entering all information, select the **OK** button.

Once you have successfully entered your new password, another dialog box will appear. This box will prompt you for a SecurID passcode.

If you have already set a Personal Identification Number (PIN), generate a passcode using your SecurID card and your established PIN. Once the SecurID card has generated a passcode, enter the passcode at the **SecurID Passcode** prompt. Upon entering the code correctly, your password will be changed.

If you do not have a PIN, enter the number currently showing on the SecurID card. You will then be prompted to create a PIN. From this point on, you must enter this PIN into the SecurID card to generate a SecurID passcode. Upon creating the PIN, your Kerberos password will be changed.

If you have any questions or experience any problems changing your Kerberos password, please contact NAVO MSRC User Support at 1-800-993-7677 or via E-mail to msrchelp@navo.hpc.mil. We will be happy to assist you in this process.

Open Source Solutions....cont.

are tested in parallel. Such a parallel evaluation is often inexpensive due to the hardware independence of open source code and minimal time invested by in-house staff. With such a small investment, the trial is low-risk and, if the tests are unsuccessful, the test bed can be discarded, and any hardware used in the testing process can be integrated into the current infrastructure. Often, these evaluations are successful, and the organization can incorporate the open source technology into their operations with confidence and some amount of experience gleaned from the evaluation.

A Timely Test Bed

In 1998, the VADIC team was approached by the Naval Oceanographic Office (NAVOCEANO) and NASA Goddard on behalf of the Smithsonian Institution to establish an automated SST visualization for the Smithsonian's "Earth Today" exhibit. The project was an impressive success story for the NAVO MSRC, and the exhibit won the Smithsonian's "Best Virtual Exhibition" award in 1999.

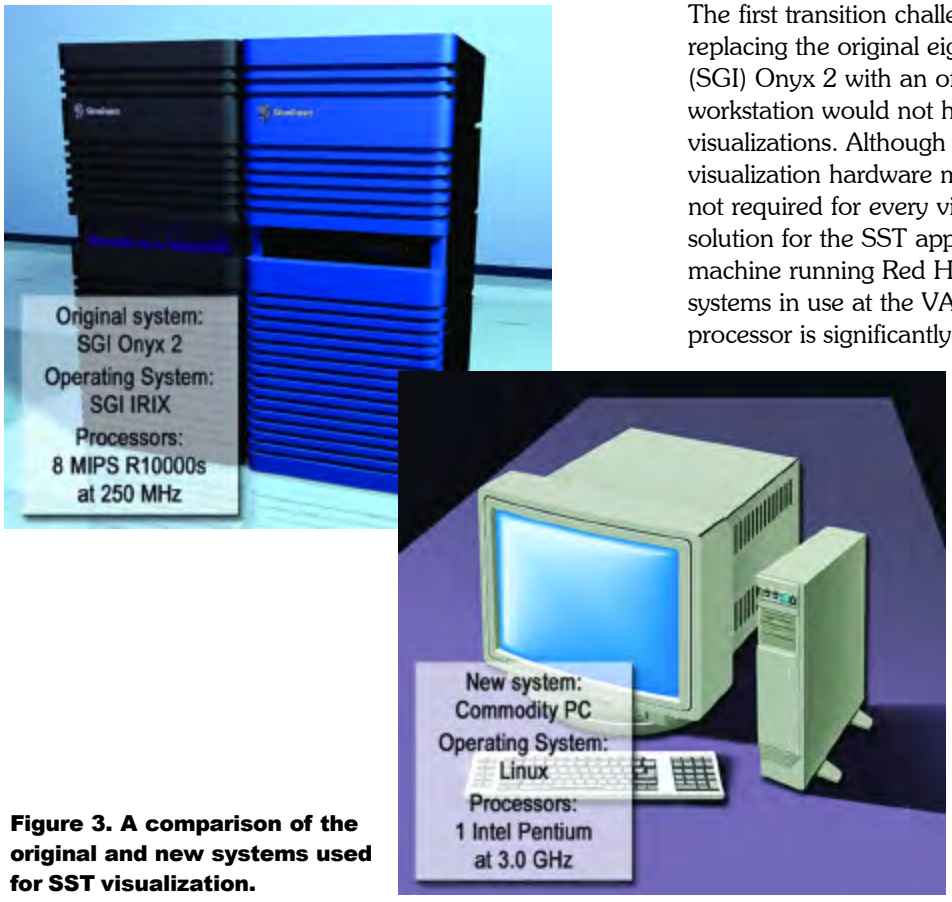

Figure 3. A comparison of the original and new systems used for SST visualization.

Data for the Smithsonian and, in fact, all SST images are acquired by satellite and processed by NAVOCEANO. When completed, a single SST image displays the surface temperature of all water on Earth. (See Figure 1, page 13.) A second image is also produced, known as SST Anomaly, which illustrates deviation in temperature from climatological averages. SST Anomaly images are often used to show the well-known "El Nino" phenomenon. (See Figure 2, page 13.)

For over 6 years, the automated process for the Smithsonian images ran every day without alteration. In late 2003, NASA Goddard again contacted the VADIC staff to request an update to the SST visualization application. NASA Goddard wanted to provide newer high-resolution imagery of the landmasses used in the SST visualizations supplied to the Smithsonian. This request coincided with the VADIC staff's research into replacing the legacy system with an open source-based approach. With this NASA Goddard request, it seemed the ideal time to update the entire SST procedure and transition to a new system. However, there were obstacles to overcome.

The Open Source Transition

The first transition challenge would be to determine that replacing the original eight-processor Silicon Graphics, Inc. (SGI) Onyx 2 with an off-the-shelf or commodity workstation would not hinder the production of SST visualizations. Although SGI is still one of the leaders in the visualization hardware market, this specialized hardware is not required for every visualization application. The best solution for the SST application was an Intel-based machine running Red Hat Linux. While the current Linux systems in use at the VADIC have a single processor, this processor is significantly faster than the VADIC SGI processors. Another major advantage was that switching to commodity hardware with an open source operating system reduces maintenance and operating costs by a factor of 10. (See Figure 3.)

The next challenge was to transition the SST visualization application to the Linux system. The original application utilized Maya®, high-end rendering and animation software, for a significant portion of the process.

Continued Next Page...

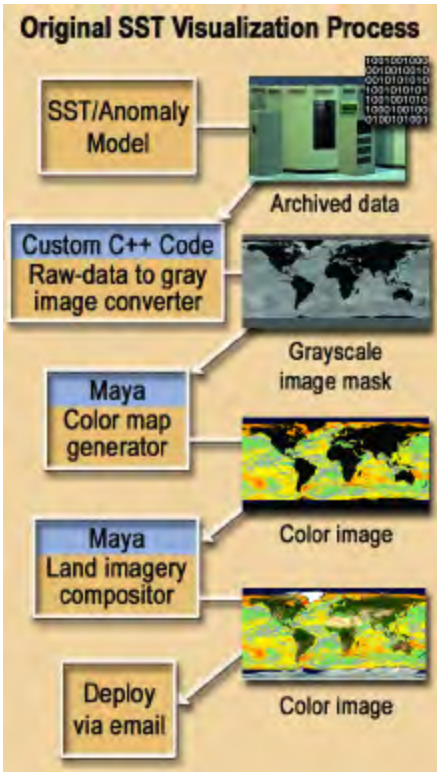

Figure 4. (Left) The original SST visualization process first uses a custom data converter written in C++ to convert raw temperature data to a 256-level grayscale image. The lowest temperatures are represented by darker grays, and the higher temperatures by brighter whites. A similar representation is used for below-average and above-average anomaly values. Maya® can import such a grayscale image, where each grayscale value can be mapped to a color. Since no actual temperature values correspond to land, it is left black. Maya® performs a procedure known as compositing, which overlays NASA's land imagery, but only in the black areas. An example of the resultant image is shown after each step of the process.

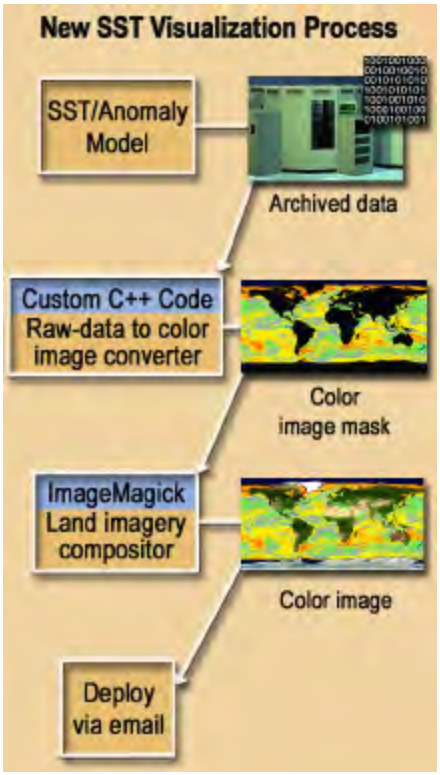

Figure 5. (Right) The new SST visualization process utilizes an updated data converter that also performs color mapping and uses ImageMagick to composite the land imagery. An example of the resultant image is shown after each step of the process.

```
? composite -compose minus sst_original.tif land_only.tif land_removed.tif
? composite -compose multiply nasa_imagery.tif land_only.tif land_imagery.tif
? composite -compose plus land_imagery.tif land_removed.tif final_image.tif
```

Figure 6. An example of ImageMagick commands used to composite the original SST image with the NASA imagery to produce the final image. These three commands replace Maya® for the entire compositing process.

One option was to simply buy or transfer licenses to Linux. This would produce a fast, painless transition. However, Maya's capabilities far exceed the requirements for the SST visualization application. Since the application required modification to accommodate NASA Goddard's new land imagery request, there was another alternative.

The application could be rewritten to use open source software tools rather than Maya®. This required revising the color mapping and compositing steps in the visualization process. First, the raw-data converter was redesigned to act as the new color-mapping system. This was a simple modification to the source code: rather than translating the data into gray values from 0 to 256, and then into color values, VADIC programmers directly mapped the raw data to the color values. Replacing the proprietary SGI MIPSpro compiler was an essential step in this transition. The data conversion code was ported to the GNU C++ compiler on Linux, and then the color mapping modifications were added.

The heart of the application transition, however, was the switch from Maya® to ImageMagick to composite the land imagery. ImageMagick is an open source collection of image manipulation tools that, if desired, can be grouped together into scripts for automated processing. VADIC programmers were able to combine a set of ImageMagick commands that performed the exact same compositing routine as Maya®. Figure 4 depicts the old SST image process, while Figure 5 depicts the new process, utilizing the new converter and ImageMagick. Figure 6 is an example of the ImageMagick compositing commands.

Since ImageMagick is an open source software, it was a very attractive alternative to Maya®. While it cannot replace Maya® for every project, ImageMagick eliminated the software licensing issues and replaced the image generation functionality for this project. With the migration now completed, the result is a nearly equivalent system in which the hardware is a fraction of the cost, the operating system is inexpensive, and the tools are free.

Acknowledgements

We would like to acknowledge Russell Daines of Lockheed Martin Space Operations for his modifications to the source code and implementation of the ImageMagick scripts.

2004 EVENTS

April 21 - 22
MIT IT Conference
Cambridge, MA
http://ilp-www.mit.edu/events/IT2004/

May 6 - 7
Third Virtual Machine Research and Technology Symposium (VM '04)
San Jose, CA · www.usenix.org/events/vm04/

May 24 - 26
Grid Today 2004 (Gt04)
Philadelphia, PA
www.gridtoday.com/04/conference/

June 7
CLADE 2004: Workshop on the Challenges of Large Applications in Distributed Environments
Honolulu, HI · www.caip.rutgers.edu/clade2004/

June 11-13
ACM SIGPLAN Conference on Languages, Compilers, and Tools for Embedded Systems
Washington, DC · http://lctes04.flux.utah.edu

June 13
10th Workshop of Job Scheduling Strategies for Parallel Processing (JSSPP)
New York, NY
www.cs.huji.ac.il/~feit/parsched/parsched04.html

July 7 - 9
ICPADS 2004: The 10th International Conference on Parallel and Distributed Systems
Newport Beach, CA · www.cacs.louisiana.edu/icpads2004/

July 27 - 29
On the Use of Commodity Clusters for Large-Scale Scientific Applications 2004
Tysons Corner, VA · www.arl.hpc.mil/Clusters2004/

August 9 - 13
13th USENIX Security Symposium
San Diego, CA · www.usenix.org/sec04/

Sept. 20 - 23
Cluster2004: IEEE International Conference on Cluster Computing
San Diego, CA · http://grail.sdsc.edu/cluster2004/

Sept. 28 - 30
Eighth Annual Workshop on High Performance Embedded Computing
Lexington, MA · www.ll.mit.edu/HPEC/#

Oct. 6 - 9
Grace Hopper '04: Grace Hopper Celebration of Women in Computing 2004 Conference
Chicago, IL · www.gracehopper.org/

Oct. 10 - 15
Vis 2004
Austin, Texas · http://vis.computer.org/vis2004/cfp/

Nov. 6 - 12
SC2004
Pittsburgh, PA · www.sc-conference.org/sc2004/

NAVAL OCEANOGRAPHIC OFFICE * MAJOR SHARED RESOURCE CENTER
1002 Balch Boulevard . Stennis Space Center, Mississippi . 39522